The same relations are also valid for a metallic inner cylinder and the H-wave polarization, as well as for a dielectric inner cylinder and both polarizations, with the changes which are referred to in the relative sections.

REFERENCES

[1] A. Sebak, H. A. Ragheb, and L. Shafai, "Plane wave scattering by dielectric elliptic cylinder coated with nonconfocal dielectric," *Radio Sci.,* vol. 29, pp. 1393–1401, Nov./Dec. 1994.

[2] A. R. Sebak, "Electromagnetic scattering by two parallel dielectric elliptic cylinders," *IEEE Trans. Antennas Propagat.,* vol. 42, pp. 1521–1527, Nov. 1994.

[3] J. A. Stratton, *Electromagnetic Theory.* New York: McGraw-Hill, 1941.

[4] P. M. Morse and H. Feshbach, *Methods of Theoretical Physics.* New York: McGraw-Hill, 1953.

[5] H. A. Ragheb, L. Shafai, and M. Hamid, "Plane wave scattering by a conducting elliptic cylinder coated by a nonconfocal dielectric," *IEEE Trans. Antennas Propagat.,* vol. 39, pp. 218–223, Feb. 1991.

[6] J. A. Roumeliotis, H. K. Manthopoulos, and V. K. Manthopoulos, "Electromagnetic scattering from an infinite circular metallic cylinder coated by an elliptic dielectric one," *IEEE Trans. Microwave Theory Tech.,* vol. 41, pp. 862–869, May 1993.

[7] J. A. Roumeliotis and S. P. Savaidis, "Cutoff frequencies of eccentric circular-elliptic metallic waveguides," *IEEE Trans. Microwave Theory Tech.,* vol. 42, pp. 2128–2138, Nov. 1994.

[8] ——, "Scattering by an infinite circular dielectric cylinder coating eccentrically an elliptic metallic one," *IEEE Trans. Antennas Propagat.,* vol. 44, pp. 757–763, May 1996.

Enhancements of the Spectral-Domain Approach for Analysis of Microstrip Y-Junction

B. L. Ooi, M. S. Leong, P. S. Kooi, and T. S. Yeo

***Abstract*— Some enhancements of the spectral-domain approach in the polar coordinate are described. A simple and efficient algorithm is devised to numerically evaluate the contribution of the oscillatory tail of the two-dimensional (2-D) Sommerfeld integral. For the first time, four new vectorized basis functions are proposed. Good agreement is obtained between the simulated results and the measured data for a microstrip Y-junction in the 4–12 GHz range.**

***Index Terms*—Microstrip, numerical integration, planar transmission lines, spectral-domain method.**

I. INTRODUCTION

The numerical computation of the Sommerfeld integrals in the polar coordinate has been dealt with by many authors [1], [2]. In 1992, Dvorak *et al.* [1], [2] have developed some methods to compute the two-dimensional (2-D) Sommerfeld integrals in the polar coordinate. Their methods have certain drawbacks in that: 1) there is a large amount of analytical manipulation that ought to be done before the tails of the 2-D Sommerfeld integrals can be evaluated and 2) the evaluation of the tails of the 2-D Sommerfeld integrals often involves tedious and complicated functions which are not applicable for any arbitrary basis functions. Although the fast Fourier transform (FFT) algorithm [3] can be used to improve the convergence of the Sommerfeld integrals for the modeling of nonrectangular discontinuity, the FFT algorithm fails to achieve good solution because the discretization scheme cannot assure that all points are located in the cross-points of a regular grid. Moreover, the modeling of a nonrectangular discontinuity with rectangular cells is ineffective because the use of a large number of elements is necessary.

Of course, the Rao's vector basis function [4] can always be used to eliminate the staircase approximation. However, this basis function is not very competitive as compared to the rectangular basis function and should be used only if it is absolutely necessary. In 1993, Eibert [6] provided an enhancement on Rautio's basis function [5] by using a new expansion function consisting of one triangle and two adjacent rectangles with arbitrary orientation within the plane of the circuit. In his method, a removable singularity, which requires extra analytical manipulations, appears in the Fourier transform of a linear distribution with triangular support [7] when the polar transform vector $\lambda = \sqrt{k_x^2 + k_y^2}$ is perpendicular or parallel to any edge of the triangle [8].

The purpose of this paper is to introduce some enhancements of the spectral-domain approach and to use four new vectorized expansion functions based on an extension on Eibert's work, for the analysis of an arbitrarily angled microstrip Y-junction. This paper further describes a new general algorithm for evaluating the 2-D polar spectral integrals which arise. Finally, some numerical results will be presented and discussed.

II. GENERAL FORMULATIONS

An arbitrarily angled microstrip Y-junction consisting of a thickness h and a lossless nonmagnetic relative dielectric permittivity ε_r is shown in Fig. 1. The global coordinate system with the u-direction being along the arm and the v-direction being orthogonal to the u-direction, is also presented in Fig. 1.

In our analysis, four types of current expansion functions are utilized in the method. They are the arbitrarily oriented pseudo-exponential window traveling wave (PEW) functions, the vectorized roof-top subdomain functions (T), the arbitrarily oriented rectangular subdomain functions (R) and the vectorized triangular–rectangular subdomain functions (RT).

A. Arbitrarily Oriented Pseudo-Exponential Window Traveling Wave (PEW)

This current expansion function is an extension of Cicchetti's work [9] to the case of arbitrary orientation. The Fourier transforms of the basis functions can be obtained by application of linear coordinate transformations and shifting property of Fourier transform to the direct solutions of the Fourier integrals [9] for the corresponding functions which are rotated and shifted to an appropriate location within the xy-plane. The PEW, which is used to simulate the incoming and outgoing currents on the feedlines, allows us to extract the scattering parameters without any de-embedding since the scattering parameters are embedded in the coefficients of the traveling wave functions.

Manuscript received March 8, 1996; revised June 20, 1997.

The authors are with the Department of Electrical Engineering, National University of Singapore, Singapore.

Publisher Item Identifier S 0018-9480(97)07115-9.

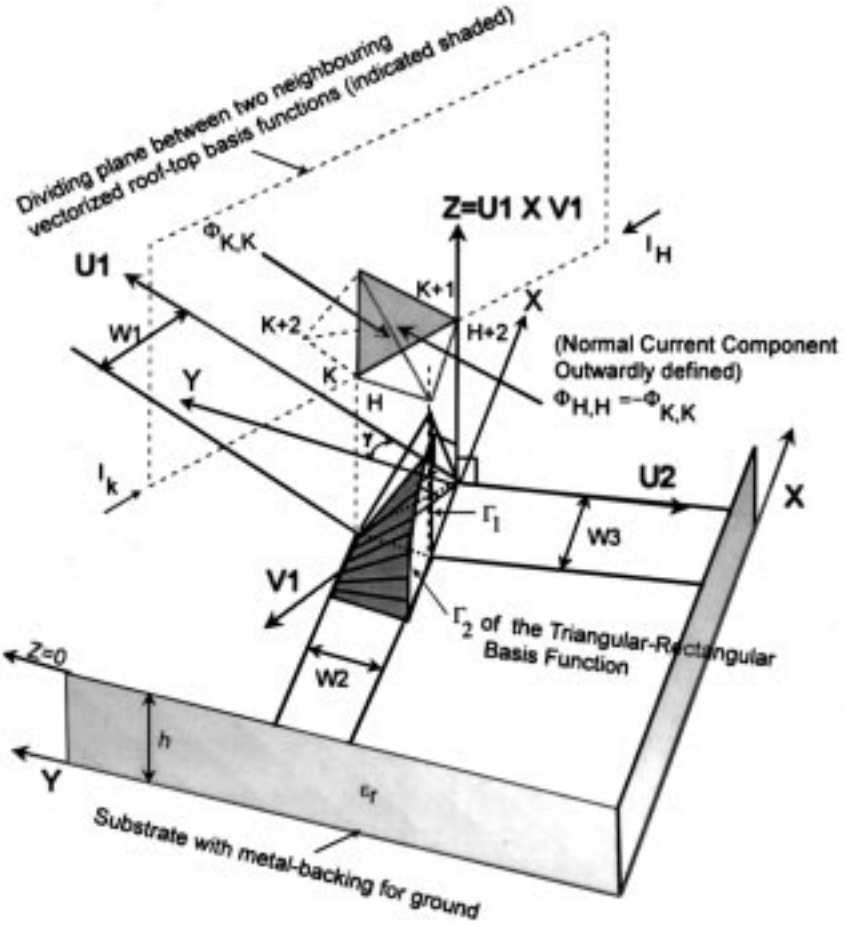

Fig. 1. A cross-sectional view of a microstrip Y-junction with two of the basis functions—namely, the vectorized roof-top basis function and the triangular-rectangular basis function. As in [8], the right-hand rule is adopted in the derivation of both basis functions, and the interior edge of the roof-top function is not a constant as compared to [4].

B. Vectorized Roof-Top Subdomain Functions (T)

Together with [8], we expand the current into the transverse and normal components along the edges of the triangle, and by combining the appropriate normal current on one side with the neighboring cell, the resultant Fourier transform of our new expression is shown in (1) at the bottom of the page, where $\overline{I}_j$ with $j = k,\ H$ is the vector along edge k or H (see Fig. 1), respectively, $\Phi_{k,\,k}$ is the unknown normal current component along edge k to edge $(k+1)$, respectively, $\overline{r}_{k+1}$is the position vector of the $(k+1)$th vertex, A is the area of the triangle, the symbol dot and cross denote, respectively, the dot and vector product, $\overline{\lambda}$ is the transform vector, and j_n denotes the spherical Bessel function of the first kind of order n. This resultant expansion function is mainly used in the overlap of the two arms of the Y-junction.

C. Arbitrarily Oriented Rectangular Subdomain Functions (R)

The mathematical expressions of the Fourier transforms of the u-direction and the v-direction of the arbitrarily oriented rectangular

$$
\begin{aligned}
&\tilde{J}_{\mathrm{T}}(\overline{\lambda};\,\overline{r}_{k+1}) \\
&= \left(\frac{\Phi_{k,\,k}}{\hat{z}\bullet\hat{I}_k\times\hat{I}_{k+2}}\right)\hat{I}_{k+2} * \left\{\frac{\hat{z}\times\overline{I}_{k+1}}{2A}\bullet\left[\frac{1}{|\overline{\lambda}|^2}\sum_{n=1}^{3} e^{j\overline{\lambda}\bullet(\overline{r}_n+\overline{r}_{n+1})/2} * \left(\left\{\overline{z}\times\overline{I}_n\left[\frac{j(\overline{r}_n+\overline{r}_{n+1})}{2} - j\overline{r}_{k+1} - \frac{2\overline{\lambda}}{|\overline{\lambda}|^2}\right]\hat{z}\bullet\overline{I}_n\times\overline{\lambda}\right\}\right.\right. \\
&\qquad \left.\left.\cdot\, j_o\left(\frac{\overline{\lambda}\bullet\overline{I}_n}{2}\right) - \overline{I}_n\frac{\hat{z}\bullet\overline{I}_n\times\overline{\lambda}}{2}\,j_1\left(\frac{\overline{\lambda}\bullet\overline{I}_n}{2}\right)\right)\right]\right\} - \left(\frac{\Phi_{k,\,k}}{\hat{z}\bullet\hat{L}_H\times\hat{L}_{H+1}}\right)\hat{L}_{H+2} \\
&\qquad \cdot\left\{\frac{\hat{z}\times\overline{L}_{H+2}}{2A}\bullet\left[\frac{1}{|\lambda|^2}\sum_{n=1}^{3} e^{j\overline{\lambda}\bullet(\overline{r}_n+\overline{r}_{n+1})/2}\left(\left\{\hat{z}\times\overline{L}_n + \left[j\,\frac{(\overline{r}_n+\overline{r}_{n+1})}{2} - j\overline{r}_{k+1} - \frac{2\overline{\lambda}}{|\overline{\lambda}|^2}\right]\hat{z}\right.\right.\right. \\
&\qquad \left.\left.\left.\bullet\,\overline{L}_n\times\overline{\lambda}\right\} * j_o\left(\frac{\overline{\lambda}\bullet\overline{L}_n}{2}\right) - \overline{L}_n\frac{\hat{z}\bullet\overline{L}_n\times\overline{\lambda}}{2}\,j_1\left(\frac{\overline{\lambda}\bullet\overline{L}_n}{2}\right)\right)\right]\right\}, \qquad (1)
\end{aligned}
$$

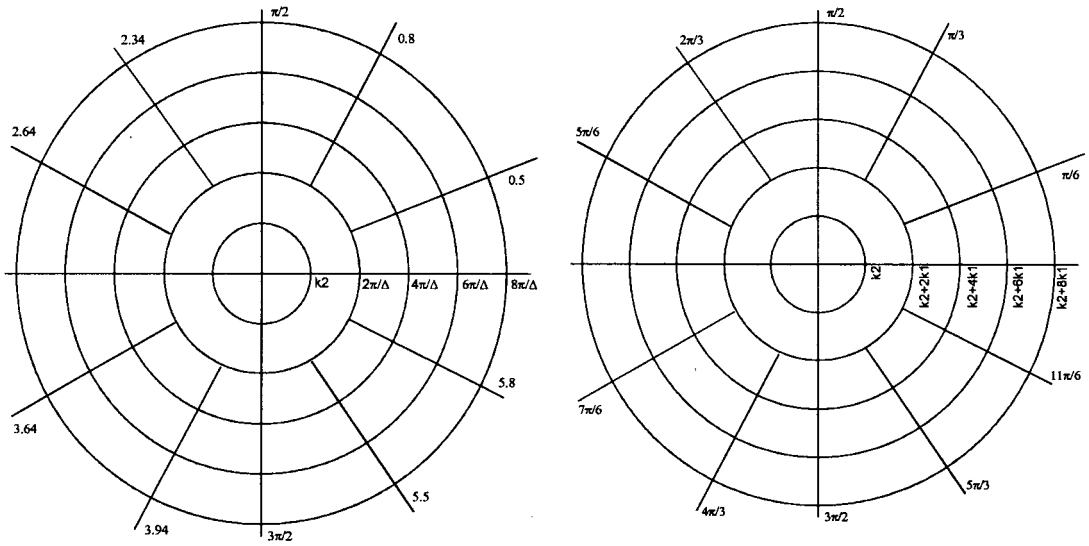

(a) (b)

Fig. 2. Partitioning of the (λ, θ) space in new scheme for numerical integration. (a) Δ is the width of the rectangular subdomain function. (b) Numerical scheme for triangular and PEW testing reaction.

subdomain function are given as

$$\tilde{J}|_{\mathrm{R}_U} = \frac{2k_e e^{j\lambda[\cos(\theta+\gamma)v_o+\sin(\theta+\gamma)u_o]}(\hat{x}\,\sin\gamma+\hat{y}\,\cos\gamma)}{\sin(k_e d)} * \left\{\frac{\cos(k_e d)-\cos[\lambda d\,\sin(\theta+\gamma)]}{[\lambda\,\sin(\theta+\gamma)]^2-k_e^2}\right\} \cdot b\,\mathrm{sinc}\left\{\frac{b}{2}\lambda\,\cos(\theta+\gamma)\right\} \tag{2a}$$

$$\tilde{J}_{\mathrm{R}_V} = \frac{2e^{j\lambda[\cos(\theta+\gamma)v_o+\sin(\theta+\gamma)u_o]}k_e(\hat{x}\,\sin\gamma+\hat{y}\,\cos\gamma)}{\sin(k_e d)} * \left\{\frac{\cos(k_e d)-\cos[\lambda\,\cos(\theta+\gamma)d]}{[\lambda\,\cos(\theta+\gamma)]^2-k_e^2}\right\} \cdot b\,\mathrm{sinc}\left\{\frac{b}{2}\lambda\,\cos(\theta+\gamma)\right\} \tag{2b}$$

where $\theta = \tan^{-1}(k_y/k_x)$, k_e is a constant used to describe the shape of the piecewise sinusoidal function and must be less than $\pi/2d$ to avoid a dip at the center, d is longitudinal length of the basis function, and b is the width of the basis function. This expansion function is utilized in the vicinity of the microstrip transition on the three feedlines. The overlap on the feedline between the area covered by this expansion functions and that of the PEW's accounts for the higher order modes in the vicinity of the discontinuities.

D. Vectorized Triangular–Rectangular Subdomain Functions (RT)

Using the same approach as in Section II-B, the Fourier transform of the vectorized triangular–rectangular subdomain function (See Fig. 1) is given as

$$\tilde{J}_{\mathrm{RT}} = \frac{\Phi_{k,k}\hat{I}_{k+2}}{\hat{z}\bullet\hat{I}_k\times\overline{I}_{k+2}}\left[\frac{\hat{z}\times\overline{I}_{k+1}}{2A}\bullet\sum_{n=1}^{3}\frac{e^{j\overline{\lambda}\bullet(\overline{r}_n+\overline{r}_{n+1})/2}}{|\overline{\lambda}|^2}\cdot\left(\left\{\hat{z}\times\overline{I}_n+\left[j\frac{(\overline{r}_n+\overline{r}_{n+1})}{2}-j\overline{r}_{k+1}-\frac{2\overline{\lambda}}{|\overline{\lambda}|^2}\right]\hat{z}\bullet\overline{I}_n\times\overline{\lambda}\right\}j_o\left(\frac{\overline{\lambda}\bullet\overline{I}_n}{2}\right)-\overline{I}_n\,\frac{\hat{z}\bullet\overline{I}_n\times\overline{\lambda}}{2}\,j_1\left(\frac{\overline{\lambda}\bullet\overline{I}_n}{2}\right)\right)\right], \quad \overline{r}\in\Gamma_1$$

$$= \frac{k_e b\Phi_{k,k}e^{j\lambda[\cos(\theta+\gamma)v_o+\sin(\theta+\gamma)u_o]}}{j\lambda\,\cos(\theta+\gamma)\sin(k_e d)} \cdot\left\{\frac{\cos(k_e d)-\cos[\lambda d\,\sin(\theta+\gamma)]}{[\lambda\,\sin(\theta+\gamma)]^2-k_e^2}\right\} \cdot\left\{1-e^{j\lambda\,\cos(\theta+\gamma)v_1/2}\,\mathrm{sinc}\left[\frac{\lambda\,\cos(\theta+\gamma)v_1}{2}\right]\right\} \cdot\frac{\hat{I}_k\times\hat{I}_{k+2}\times\hat{I}_k}{|\hat{I}_k\times\hat{I}_{k+2}\times\hat{I}_k|}, \quad \overline{r}\in\Gamma_2 \tag{3}$$

where d is the longitudinal length of the ramp function, b is the horizontal width of the ramp function and $\overline{r}_{k+1}$ is the position vector of the $(k+1)$ edge [8]. This basis function is applied consecutively at the junction of each feedline. For each feedline, two basis functions of opposite peak are assigned at the junction. Hence, fewer basis functions are required for the description of the current.

III. Numerical Integration

The polar representation of the electric-field integral equation (EFIE) is solved by imposing zero tangential electric field on the microstrip surface $(z = 0)$ and using the Galerkin's method. With the above current basis functions, we obtained a matrix given as

$$[Z][I] = [V] \tag{4}$$

where the elements of $[Z_{ij}]$ are the double integral reaction between the basis function i and the testing function j. The double infinite integration in each matrix element is carried out numerically. For the integration with respect to λ, the infinite integration is divided into three regions, namely:

1) $0 < \lambda \le k_o$;
2) $k_o < \lambda < k_2$;
3) $\lambda \ge k_2$.

This partitioning is essential so as to separately cater for the poles that are found in Region 2.

In the interval $0 < \lambda \le k_0$ and $0 \le \theta \le 2\pi$, the impedance matrix elements $[Z_{RR}]$ along the x- or y-axis are smoothed with the change of variable $\lambda = \cos t$. As for the reaction between the u-direction and either the x- or y-direction, and the reaction

TABLE I
NUMERICAL RESULTS OBTAINED BASED ON THE NEW SCHEME AS ILLUSTRATED IN FIG. 2(a). THIS IS EVALUATED FOR THE CASE WHEN $\varepsilon_r = 2.32$ AND $h = 1.56e^{-3}$m WITH THE BASIS-TESTING SEPARATION AT $1.5\lambda_g$

Range (λ,θ)	Number of Points Taken in (λ,θ)	Result obtained at Frequency =2 GHz	Result obtained at Frequency= 20 GHz
$\left(\left[k_2, \frac{2\pi}{\Delta}\right], \left[0, \frac{\pi}{2}\right]\right)$	(16,16)	-j5.00831276763e-5	j9.584855433949e-6
	(32,32)	j1.06831394644e-5	j9.584855433949e-6
	(48,48)	j1.07340144805e-5	j9.723320904687e-6
	(64,64)	j1.07462308335e-5	j9.753022731345e-6
	(100,100)	j1.07463183369e-5	j9.753689599759e-6
	(300,300)	j1.07469298424e-5	j9.755320357554e-6
$\left(\left[\frac{2\pi}{\Delta}, \frac{4\pi}{\Delta}\right], [0, 0.5]\right)$	(32,32)	-j6.358854081062e-6	-j2.020940351984e-7
	(48,48)	-j7.472454749057e-6	-j3.939656856559e-7
	(64,64)	-j7.483015819895e-6	-j3.950004909307e-7
	(128,128)	-j7.487845355880e-6	-j3.955174263660e-7
	(500,500)	-j7.488151004668e-6	-j3.955503329840e-7
$\left(\left[\frac{2\pi}{\Delta}, \frac{4\pi}{\Delta}\right], [0.5, 0.8]\right)$	(16,16)	-j1.613049301819e-6	j2.172322054908e-7
	(32,32)	-j2.432027030572e-6	j1.797882833436e-7
	(48,48)	-j2.451089240217e-6	j1.779770447757e-7
	(64,64)	-j2.453757936698e-6	j1.777074872291e-7
	(128,128)	-j2.454823670427e-6	j1.775968884887e-7
	(500,500)	-j2.454890191107e-6	j1.775898447643e-7
$\left(\left[\frac{2\pi}{\Delta}, \frac{4\pi}{\Delta}\right], \left[0.8, \frac{\pi}{2}\right]\right)$	(16,16)	-j4.291152099911e-6	-j1.6323213417691e-7
	(32,32)	-j6.415473550057e-6	-j4.6299322161084e-7
	(48,48)	-j6.473871211706e-6	-j4.6805518021162e-7
	(64,64)	-j6.482579412394e-6	-j4.6882622922708e-7
	(128,128)	-j6.486153799224e-6	-j4.6914495093147e-7
	(500,500)	-j6.486381508345e-6	-j4.6916535009123e-7
$\left(\left[\frac{4\pi}{\Delta}, \frac{6\pi}{\Delta}\right], [0, 0.5]\right)$	(16,16)	j3.079697153420e-7	j2.664257100184e-8
	(32,32)	-j2.582685177857e-8	-j1.88637623586e-11
	(48,48)	-j2.701572983423e-8	-j1.146286886692e-10
	(64,64)	-j2.716579829537e-8	-j1.267939671978e-10
	(500,500)	-j2.722735273534e-8	-j1.318052992510e-10
$\left(\left[\frac{4\pi}{\Delta}, \frac{6\pi}{\Delta}\right], [0.5, 0.8]\right)$	(16,16)	-j1.024911413874e-7	-j1.2650219858427e-8
	(32,32)	j3.5144340112211e-9	-j2.4108362296808e-9
	(48,48)	j6.1228238905795e-9	-j2.1842016185366e-9
	(64,64)	j6.5174842880371e-9	-j2.1502068383963e-9
	(128,128)	j6.6811298931402e-9	-j2.1361594729587e-9
	(500,500)	j6.6916428415043e-9	-j2.1352592200791e-9
$\left(\left[\frac{4\pi}{\Delta}, \frac{6\pi}{\Delta}\right], \left[0.8, \frac{\pi}{2}\right]\right)$	(16,16)	-j2.0903686146733e-8	-j7.3137548460316e-9
	(32,32)	-j4.4618064799546e-7	-j3.9325073434912e-8
	(48,48)	-j4.0634276662564e-7	-j3.5601413830717e-8
	(64,64)	-j4.0176081808443e-7	-j3.5240859609734e-8
	(128,128)	-j4.0000747231716e-7	-j3.5105795744503e-8
	(500,500)	-j3.9990060951296e-7	-j3.5097655396569e-8

between the v-direction and either the x- or y-direction, $\lambda = \sin t$ should be used instead. For the mutual reaction between the u itself or v itself, $\lambda = \cosh t$ has to be used. These transformations are used to smoothen the infinite derivative of the Green functions. Since the variation along this region is slow as compared to Regions 2 and 3, a simple 2-D Gaussian quadrature of 64 points is sufficient to span through the whole spectrum of the frequency range.

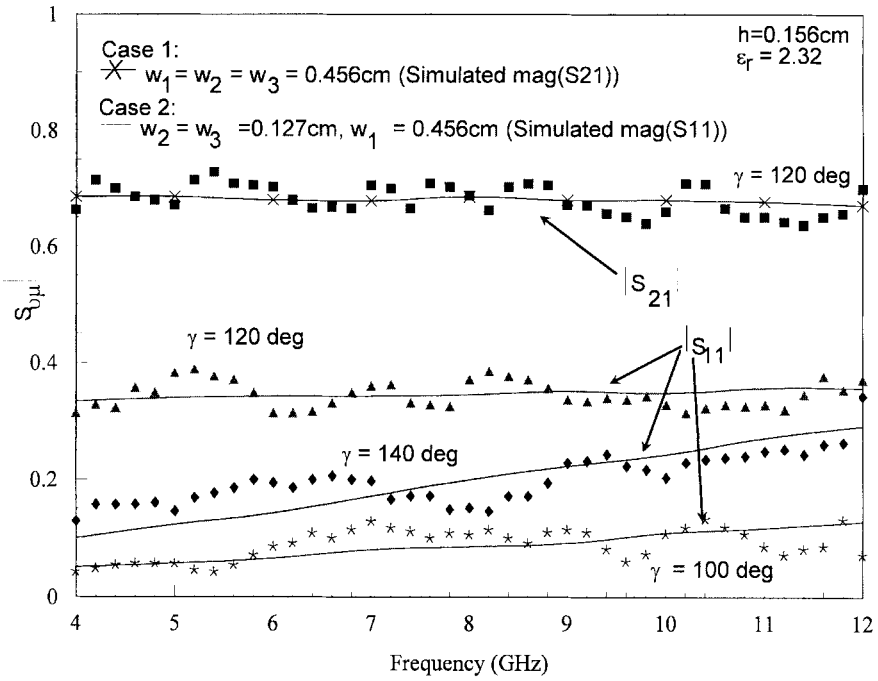

Fig. 3. Comparison of $S_{\mu v}$ measured data [13] (symbols square, diamond, asterisk, and triangle) and simulated results (dash and solid lines) from the new numerical scheme for various Y-junction angles γ.

In the interval $k_o < \lambda < k_2$ and $0 \leq \theta \leq 2\pi$, the singularity is extracted using the method proposed in [11]. With the substitution $\lambda = \cosh t$ and the methods proposed in [11], one can integrate the smoother integrand with a 64-point Gaussian quadrature for both the λ and θ variables.

The integrand in the interval $\lambda \in [k_2, \infty]$ is a slowly converging oscillating function over a semi-infinite interval. The integrand in the θ direction is also an oscillating function of frequency proportional to λ. Most methods (as proposed in the literature) have omitted this oscillation of the integrand in the θ direction. In 1994, Cai [12] has suggested a new method to evaluate this 2-D spectral integral. In his method, the integrand region in the λ direction is divided into several subregions: $\lambda = 0, \lambda_o, 2\lambda_o, 3\lambda_o, \cdots, n\lambda_o$. Within each subregion between $(n-1)\lambda_o$ and $n\lambda_o$, it is further divided into n sub-subregions in the θ direction, where $n = 1, 2, 3, \cdots$. Finally, $(k \times m)$ sampling points are subsequently applied in each sub-subregion.

Since the integrand is a decaying function, this partition is not efficient. We have instead adopted that as illustrated in Fig. 2(a) for the rectangular testing reaction and Fig. 2(b) for the triangular and PEW testing reaction. There, Δ is the width of the rectangular subdomain functions. From the impedance matrix, it is noted that the integrand of the off-diagonal matrix elements becomes more highly oscillatory as the separation distance between the basis function and testing function increases. Also, as the frequency increases, the integrand of the matrix elements becomes more oscillatory. Thus, if a dedicated quadrature is devised to accurately solve the impedance matrix elements located furthest from the diagonal and at the highest frequency of interest, say $f_{\max}$, it should equally be able to accurately evaluate the remaining matrix elements at any frequencies below $f_{\max}$. This implemented numerical scheme results in a major improvement in the computation time as the same set of dedicated weights and abscissas can be used over and over again for the same type of integrand. In our approach, the 64-point Simpson's method is selected. The infinite integral is truncated at a large distance of approximately $(k_2 + 12k_0)$ away, where its contribution to the solution of the integrand is relatively insignificant.

IV. Results and Discussions

Table I presents a typical set of numerical results of the matrix element $[Z_{RR}]$ in (4) for the interval $\lambda \in [k_2, 8\pi/\Delta]$ under the new scheme. The depicted range of integration is only for a quadrant of Fig. 2(a). From Table I, a 64-point Simpson's formula is observed to be the most appropriate one to cater for the whole spectrum of frequency as the numerical results obtained at both 2 and 20 GHz converge. For instance, for a range of (λ, θ) of $([2\pi/\Delta, 4\pi/\Delta], [0.8, \pi/2])$, the numerical results for $[Z_{RR}]$ have converged to within three significant digits as the number of points taken in (λ, θ) increases from (16, 16) to (64, 64). Similar trends have also been noted for the other types of integrands, but these will not be reproduced here for brevity.

Fig. 3 presents the magnitude of the scattering parameters $S_{\mu v}$ of two symmetric Y-junctions as a function of frequency in the range 4–12 GHz, for Y-junction angles γ of 100, 200, and 140°. They are namely for: 1) Case 1: $w_1 = w_2 = w_3 = 0.456$ cm and 2) Case 2: $w_1 = 0.456$ cm, $w_2 = w_3 = 0.127$ cm. Excellent agreement between the measured data obtained from [13] (denoted as symbols) and the simulated results (dashed and solid lines) is noted. Close agreement has also been obtained for a known T-junction structure, but due to space constraints it is not reproduced here.

V. Conclusion

For the first time, four new vectorized basis functions are formulated and applied in the spectral-domain analysis of a Y-junction. A simple and efficient algorithm is also proposed to solve the 2-D Sommerfeld integral. Good agreement between the numerical results and the measured data found in [13] has been obtained.

References

[1] S. L. Dvorak, "Numerical computation of 2-D Sommerfeld integrals—Decomposition of the angular integral," *J. Comput. Phys.*, vol. 98, pp. 199–216, 1992.

[2] ____, "Numerical computation of 2-D Sommerfeld integrals—A novel asymptotic extraction technique," *J. Comput. Phys.*, vol. 98, pp. 217–230, 1992.
[3] B. Drachman, M. Cloud, and D. P. Nyquist, "Accurate evaluation of Sommerfeld integrals using the fast Fourier transform," *IEEE Trans. Antennas Propagat.*, vol. 37, pp. 403–406, Mar. 1989.
[4] S. M. Rao, D. R. Wilton, and A. W. Glisson, "Electromagnetic scattering by surfaces of arbitrary shape," *IEEE Trans. Antennas Propagat.* vol. AP-30, pp. 409–418, May 1982.
[5] J. C. Rautio, "Triangular cells in an electromagnetic analysis of arbitrary microstrip circuits," in *IEEE MTT-S Dig.*, Dallas, TX, May 8–10, 1990, pp. 701–704.
[6] F. Eibert and V. Hansen, "Triangular and rectangular elements in the spectral domain analysis of arbitrarily shaped planar circuits," *IEEE Trans. Antennas Propagat.*, vol. 41, pp. 1145–1147, Aug. 1993.
[7] B. Houshmand, W. C. Chew, and S. W. Lee, "Fourier transform of a linear distribution with rectangular support and its applications in electromagnetics," *IEEE Trans. Antennas Propagat.*, vol. 39, pp. 252–254, Feb 1991.
[8] K. McInturff and P. S. Simon, "The Fourier transform of linearly varying functions with polygonal support," *IEEE Trans. Antennas Propagat.*, vol. 39, pp. 1441–1443, Sept. 1991.
[9] R. Cicchetti and A. Faraone, "An expansion function suited for fast full-wave spectral domain analysis of microstrip discontinuities," *Int. J. Microwave Millimeter-Wave Comput.-Aided Eng.*, vol. 4, no. 3, pp. 297–306, 1994.
[10] M. Kobayashi and H. Sekine, "Closed-form expressions for the current distributions on open microstrip lines," *IEEE Trans. Microwave Theory Tech.*, vol. 39, pp. 1115–1119, July 1991.
[11] B. L. Ooi, M. S. Leong, and P. S. Kooi, "A fast, accurate, and efficient method for pole extraction in microstrip problems," *Microwave Opt. Technol. Lett.*, vol. 8, no. 3, pp. 132–136, 1995.
[12] M. Cai, P. S. Kooi, and M. S. Leong, "An efficient approach for the evaluation of the double integrals in the analysis of printed circuit antennas," *Microwave Opt. Technol. Lett.*, vol. 7, no. 6, pp. 269–270, 1994.
[13] R. Mehran, "Calculation of microstrip bends and Y-junction with arbitrary angle," *IEEE Trans. Microwave Theory Tech.*, vol. MTT-26, pp. 400–405, June 1978.

Analyticity of Electromagnetic Fields in Regions Characterized by Analytic Dielectric Parameters and Analytic Sources

S. Caorsi and M. Raffetto

***Abstract*—In this paper, the analyticity of time-harmonic electromagnetic fields in regions characterized by analytic dielectric parameters and analytic sources is proven.**

***Index Terms*—Electromagnetic theory, theoretical electromagnetics.**

I. Introduction

The knowledge of the analytic behavior of the electromagnetic field is of fundamental importance for the solutions of some theoretical electromagnetic problems—typically, uniqueness problems. Thus, for example, Müller [1] proved the uniqueness of the solutions of some boundary value problems (e.g., Theorem 34) and the uniqueness of the solutions of some scattering problems (e.g., Theorem 61) by using the analyticity of the electromagnetic field in any source-free and homogeneous region. Moreover, Caorsi and Raffetto [2] proved an extension of the classical uniqueness theorem [3] for time-harmonic electromagnetic boundary value problems by using a result (proved by Müller) based again on the analyticity of the electromagnetic field in any source-free and homogeneous region.

It is important to note that the indicated applications of the analyticity of the electromagnetic field are restricted to homogeneous dielectric materials. However, many problems of physical interest, such as the spherical Luneberg lens problem [4], [5], or the study of the propagation along the old graded index optical fibers, or the reflection of electromagnetic waves from continuously stratified media [6], or even the theory of Maxwell's "fish-eyes" lens [4], involve materials with continuously varying dielectric properties.

Consequently, it would be important to generalize the indicated result of analyticity to "analytically inhomogeneous" materials, i.e., to materials having (nonconstant) analytic dielectric parameters. For example, this generalization could allow further extensions of the uniqueness theorem for time-harmonic electromagnetic boundary value problems (i.e., to cases involving dielectric materials which are lossy in a part of the region of interest and "analytically inhomogeneous" and lossless in the rest of the region).

The goal of this paper is to move toward such a generalization of the analytic behavior of the electromagnetic field. In particular, it will be shown that the electromagnetic field is analytic in any open region characterized by analytic dielectric parameters and analytic sources.

II. A Result on the Analyticity of the Electromagnetic Field

In this section, we will prove our main result about the analyticity of the electromagnetic field. It is important to note that in this paper a scalar or vector field is called analytic in an open region $\Omega \subset R^3$ if it is defined in Ω and if it can be developed in multiple power series in a neighborhood of every point belonging to Ω [7, p. 212], [8, p. 170]. Then, in particular, by "analyticity of the electromagnetic field in Ω," we mean that the electric and magnetic fields can be developed in multiple power series in a neighborhood of every point belonging to Ω.

Theorem Let Ω be an open region in R^3. Moreover, let $\mathbf{E}$ and $\mathbf{H}$ be twice continuously differentiable vector fields in Ω (i.e., $\mathbf{E} \in [C^2(\Omega)]^3$ and $\mathbf{H} \in [C^2(\Omega)]^3$), such that

$$\begin{cases} \nabla \times \mathbf{E}(\mathbf{r}) = -j\omega\mu(\mathbf{r})\mathbf{H}(\mathbf{r}), & \text{in } \Omega \\ \nabla \times \mathbf{H}(\mathbf{r}) = \mathbf{J}(\mathbf{r}) + j\omega\varepsilon(\mathbf{r})\mathbf{E}(\mathbf{r}), & \text{in } \Omega \end{cases} \tag{1}$$

where ω is the angular frequency (assumed to be strictly positive), $\varepsilon(\mathbf{r})$ and $\mu(\mathbf{r})$ are complex scalar fields analytic in Ω, and $\mathbf{J}(\mathbf{r})$, which represents the source of the electromagnetic field, is a complex vector field analytic in Ω.

Then $\mathbf{E}$ and $\mathbf{H}$ are analytic vector fields in Ω.

Proof: By combining both equations appearing in (1), we obtain

$$\begin{aligned} \nabla \times \left[\frac{1}{\mu(\mathbf{r})}\nabla \times \mathbf{E}(\mathbf{r})\right] &= -j\omega\nabla \times \mathbf{H}(\mathbf{r}) \\ &= -j\omega\mathbf{J}(\mathbf{r}) + \omega^2\varepsilon(\mathbf{r})\mathbf{E}(\mathbf{r}), \qquad \text{in } \Omega. \end{aligned} \tag{2}$$

By using the vector identity

$$\nabla \times (u\mathbf{V}) = \nabla u \times \mathbf{V} + u\nabla \times \mathbf{V} \tag{3}$$

Manuscript received September 27, 1996; revised June 20, 1997.

S. Caorsi was with the Department of Electronics, University of Pavia, I-27100 Pavia, Italy. He is now with DIBE–University of Genoa, 16145 Genoa, Italy.

M. Raffetto is with the Department of Biophysical and Electronic Engineering, University of Genoa, I-16145 Genoa, Italy.

Publisher Item Identifier S 0018-9480(97)07116-0.